Ionics
https://doi.org/10.1007/s11581-026-07389-z

RESEARCH

Carbon black-modified polyvinyl alcohol-based gel polymer electrolytes with enhanced ionic conductivity

A. A. Rahim[1] · C. G. Er[1] · P. Q. B. Mazlan[1] · A. R. M. Rais[1,2] · N. M. Disa[1,2] · M. H. Buraidah[3] · N. Shamshurim[4] · I. M. Noor[4,5] · M. F. Shukur[6] · M. F. Aziz[1,2]

Received: 24 February 2026 / Revised: 23 June 2026 / Accepted: 16 July 2026

Abstract
Gel polymer electrolytes (GPEs) have gained attention as safer alternatives to volatile liquid electrolytes in electrochemical systems typically in dye-sensitized solar cells (DSSCs). However, their performance is limited by their high polymer crystallinity and low ionic conductivity. In this study, a series of polyvinyl alcohol (PVA)-based GPEs system were synthesized using potassium iodide (KI) salt in ethylene carbonate (EC), propylene carbonate (PC), and dimethyl sulfoxide (DMSO) solvent. Various concentrations of carbon black (CB) nanofillers were added in electrolytes to study the effect of nanofiller on electrolyte characteristics. The structural and electrochemical properties of the GPEs was systematically investigated using X-ray diffraction (XRD), Fourier-transform infrared spectroscopy (FTIR), and electrochemical impedance spectroscopy (EIS). XRD results confirmed a reduction in crystallinity with increasing CB content, while FTIR analysis indicated strong interactions between CB and the polymer matrix. The highest ionic conductivity across all samples was 15.90 mS cm^{-1} for the PVA-based electrolyte without CB. Within the CB-doped series, conductivity increased with increasing of CB amount and reached a maximum of 11.80 mS cm^{-1} at 12 wt% CB, indicating that moderate CB loading capable to form partially percolated networks that improve ion transport relative to other CB-containing samples. The findings demonstrate that carbon black able to tune the structural and electrochemical properties of PVA-based GPEs, although the GPE without CB gave the highest absolute conductivity in this study, offering promising potential for advanced electrochemical applications.

Keywords Gel polymer electrolyte · Polyvinyl alcohol · Carbon black · Ionic conductivity · Electrochemical properties

Introduction

The growing demand for environmentally friendly and efficient energy conversion systems particularly dye-sensitized solar cells (DSSCs), has driven researchers to continuously explore innovative materials that enhance device performance while ensuring safety. In DSSCs, electrolytes facilitate iodide/triiodide (I^-/I_3^-) redox shuttling between electrodes, which is crucial for photocurrent generation and energy conversion. Although liquid electrolytes deliver high

✉ M. F. Shukur
mfadhlullah.ashukur@utp.edu.my

✉ M. F. Aziz
fareezuanaziz@usm.my

1 School of Physics, Universiti Sains Malaysia, USM, Penang 11800, Malaysia

2 Energy Studies Research Group, School of Physics, Universiti Sains Malaysia, USM, Penang 11800, Malaysia

3 Department of Physics, Faculty of Science, Centre for Ionics University of Malaya, Universiti Malaya, Kuala Lumpur 50603, Malaysia

4 Ionic Materials and Energy Devices Laboratory, Physics Department, Faculty of Science, Universiti Putra Malaysia, UPM, Serdang, Selangor Darul Ehsan 43400, Malaysia

5 Physics Division, Centre of Foundation Studies for Agricultural Science, Universiti Putra Malaysia, UPM, Serdang, Selangor Darul Ehsan 43400, Malaysia

6 Fundamental and Applied Sciences Department, Universiti Teknologi PETRONAS, Seri Iskandar, Perak 32610, Malaysia

Published online: 25 July 2026

ionic conductivity ($\sim 10^{-3} - 10^{-2}$ S cm^{-1}) [1, 2], their issues relating to leakage and flammability limits the DSSCs commercialization [2–4].

Gel polymer electrolytes (GPEs) have drawn interest as alternatives to liquid electrolytes in DSSCs as they offer enhanced safety, mechanical integrity, and flexibility [3–5]. It has been reported that the ionic conductivity of GPEs have achieved in the range of $10^{-4} - 10^{-3}$ S cm^{-1} [4, 5]. Common host polymers that have been reported in synthesis of GPE are polyvinyl alcohol (PVA), polyethylene glycol (PEO), polymethyl methacrylate (PMMA), and polyacrylonitrile (PAN) [5–7]. PVA is a semicrystalline and hydrophilic, which often used as a host polymer in GPE preparation due to its excellent chemical stability, nontoxicity and biodegradability [7, 8]. Recent GPE studies as reported by Alinejad et al. [9], the ionic conductivity of PVA-based GPE achieved at 2.45 mS cm^{-1}. However, its high crystallinity limits ionic mobility, leading to low ionic conductivity, which considered still below liquid electrolyte benchmarks and insufficient for optimal DSSC performance. These requiring modifications to provide better performance of GPEs.

Thus, to address the limitations of crystallinity in PVA matrices, various methods have been explored including addition of salts, plasticizers or additives, and nanofillers. Dopant salt in polymer electrolytes provide additional charge carriers which help to enhance electrical stability and ionic conductivity in a variety of solvents. Salt selection for the preparation of GPEs is essential for optimal electrochemical applications, with low lattice energy being significant for improved salt dissociation and ion transport. Previous studies have been used iodide salts in preparation of GPEs especially in DSSC application like potassium iodide (KI), lithium iodide (LiI), and sodium iodide (NaI) [10–12]. KI is one of the most common salts used as it has lower lattice energy of 627 kJ mol^{-1} and small cations which helps in ion dissociation [12, 13]. Previous study Aziz et al. [14], demonstrated that PVA-based GPEs with KI salt and tetramethyl ammonium iodide (TMAI), achieved optimum ionic conductivity of 7.87 mS cm^{-1}. Another PVA-based GPE system containing KI salt prepared by Rahim and Aziz [15] for DSSC application, reached maximum ionic conductivity of 12.92 mS cm^{-1}. Despite these advancements, further performance optimization for DSSC applications remains a challenge.

Incorporation of nanofillers also help reduce the crystallinity in polymer matrix. Recent literature highlights a shift toward high-performance nanocomposite PVA-based electrolytes. Previous study by Kuo et al. [16], utilized titanium dioxide (TiO_2) as nanofiller in PVA- H_3PO_4 GPE for supercapacitor reached maximum conductivity of 64.90 mS cm^{-1}. Similarly, Fan et al. [17] employed silica (SiO_2) into PVA-based GPE system for zinc-air batteries (ZABs) obtained a remarkable ionic conductivity of 57.3 mS cm^{-1}. While these metal-oxide and ceramic nanofillers have been effectively reduce crystallinity, they often increase processing complexity and material costs. In contrast, carbon black (CB) is a conductive carbon-based nanomaterial, presents a distinct advantage as a cost-efficient, chemically stable nanofiller with a high surface area [18]. Although CB is widely used in batteries and supercapacitors, its applications in DSSCs have focused primarily on counter electrodes not for electrolyte. The potential of CB to serve as a multifunctional filler within the PVA-based electrolyte itself remains significantly underexplored. It remains unclear whether CB effectively reduce PVA crystallinity and enhance iodide salt dissociation. In non-PVA system, Negi et al. [19] has been employed CB as nanofiller to polyethylene oxide (PEO) electrolytes, achieving ionic conductivity of 0.012 mS cm^{-1}.

This study aims to investigate the effects of CB loading on the structural, spectroscopic, and ionic conductivity properties of PVA-based GPEs with KI as dopant salt. To the best of our knowledge, no existing study has used CB as an internal nanofiller in KI-doped PVA-based GPEs. The results provide new insights into the role of carbon-based nanofillers in tailoring polymer electrolyte performance for electrochemical applications.

Methodology

Materials

Dimethyl sulfoxide (DMSO) was obtained from R&M Chemicals. Polyvinyl alcohol (PVA) (99% hydrolysed), ethylene carbonate (EC), propylene carbonate (PC), and carbon black (CB), and iodine (I_2) crystals were purchased from Sigma Aldrich. Potassium iodide (KI) was obtained from Univar Analytical Reagent.

Preparation of gel polymer electrolyte (GPE)

Gel polymer electrolyte (GPE) was synthesized by employed a solution-casting technique. A high-purity polyvinyl alcohol (PVA) was employed as the host polymer, potassium iodide (KI) as dopant salt, and carbon black (CB) as the nanofiller. Dimethyl sulfoxide (DMSO) was used as the solvent, while ethylene carbonate (EC) and propylene carbonate (PC) acted as plasticizers to enhance ionic mobility. EC, PC, and DMSO plays a distinct role in influencing ionic transport within the GPE system. EC and PC are both high-permittivity solvents that effectively dissolve salts and enhance ion dissociation, thereby increasing the number of free mobile ions

Table 1 Designation and composition of PVA-EC-PC- KI-CB GPE system with fixed amount of PVA (5.58 wt%, 0.2 g), KI (11.72 wt%, 0.42 g), EC (8.37 wt%, 0.3 g), PC (11.16 wt%, 0.4 g), DMSO (61.38 wt%, 2 ml), and I_2 (1.80 wt%, 0.0646 g)

Designation	CB loading (wt. %)	CB mass (g)
CB1	0	0.000
CB2	3	0.239
CB3	6	0.502
CB4	9	0.652
CB5	12	0.882
CB6	15	1.088
CB7	18	1.290

available for conduction [20]. On the other hand, DMSO is an aprotic solvent with high polarity that further assists in the dissolution of salts and polymers, promoting a homogeneous gel structure and reducing the crystallinity of the polymer matrix [21]. Their combination helps in widening the electrochemical stability window and improving the overall ionic conductivity.

Initially, 0.2 g PVA was dissolved in 2 ml of DMSO at 75 °C under agitation at 420 rpm for 20 min. Separately, in another beaker, 0.42 g of KI salt was dissolved in 2 ml of DMSO with EC 0.3 g and PC 0.4 g at 30 °C for 15 min. Both solutions were combined and stirred continuously at 80 °C for 30 min until complete dissolution. Then, CB was gradually added to the mixture at different concentrations while it was heated to 100 °C and mixed until a gel-like solution was produced. Samples were prepared with nominal CB loadings of 0, 3, 6, 9, 12, 15 and 18 wt% (designated CB1-CB7). CB wt% is reported relative to the total mass of the components, which specific CB mass for each sample is listed in Table 1. Lastly, 0.0646 g of iodine (I_2) crystals were added at 45°C for 10 min. The amount of I_2 corresponds to 10% molar ratio of the total iodide ions in KI salt. The I_2 was added to generate the I^-/I_3^- redox couple, which is relevant for electrolyte studies in DSSC systems. In this work, I_2 was used to study redox-active ion transport and electrochemical behavior of the GPE, rather than to fabricate or test complete DSSC devices. The final mixture of GPE samples were transferred into veils and cured in a desiccator to prevent contamination and ensure uniformity as shown in Fig. 1.

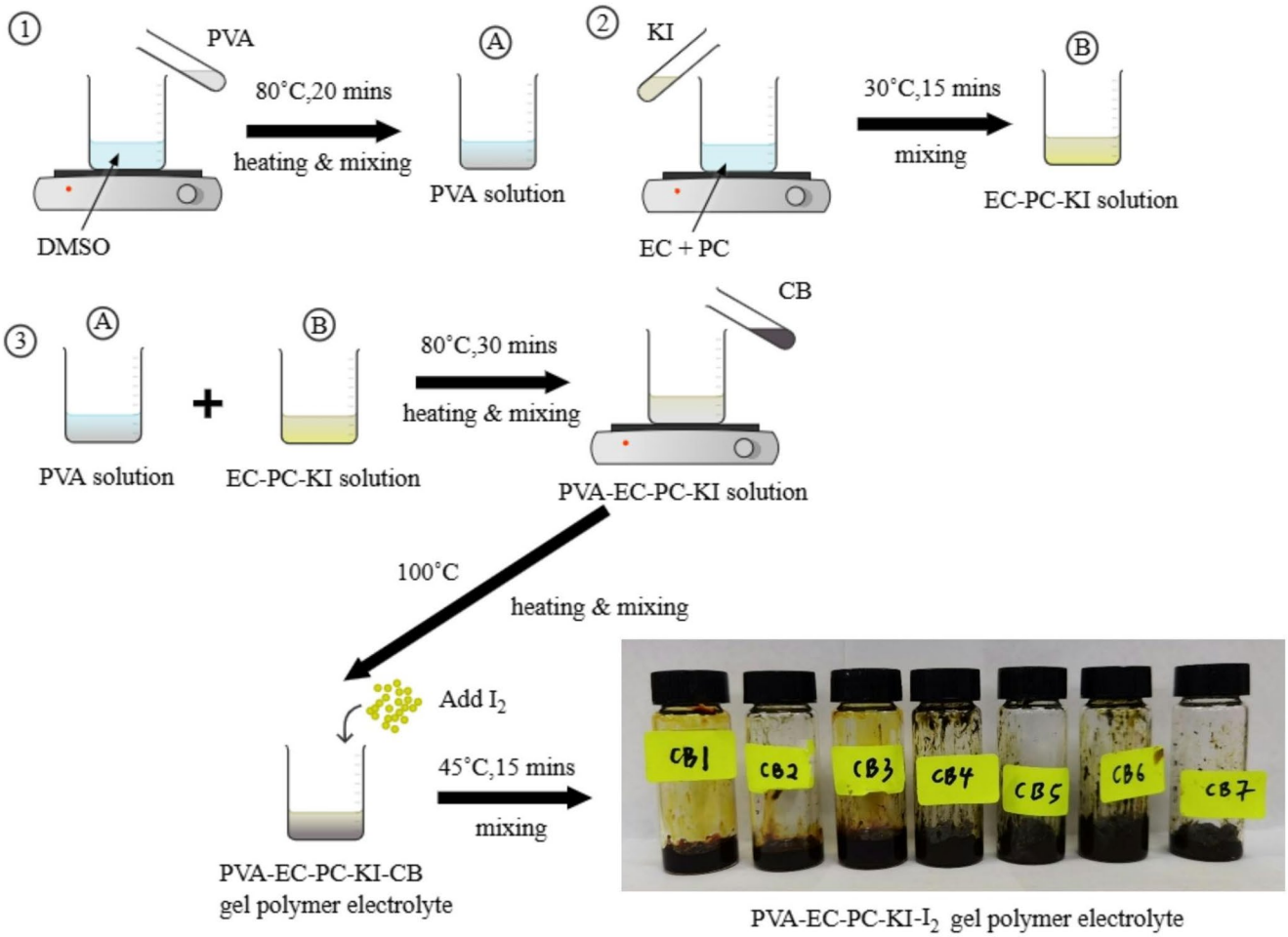

Fig. 1 Flow diagram of GPE sample preparation

Fourier transform infrared spectroscopy (FTIR)

The FTIR spectra were recorded on FTIR spectrophotometer (iS10, Thermo Scientific) with an attenuated total reflectance (ATR) attachment, allowing for direct analysis without additional sample treatment [22]. For the FTIR study, ATR crystals made of diamond are used due to their chemical inertness and durability, allowing for accurate spectral acquisition of gel polymer electrolytes without degrading the sample. This capability ensures reliable identification of functional groups and interactions within the material. Measurements were carried out in the 500–4000 cm^{-1} range with a spectral resolution of 2 cm^{-1}.

FTIR spectra were referenced with those of pure samples (PVA, KI, EC, PC, and CB), looking for shifts in peaks, differences in intensity, and new absorption bands, especially with respect to the $O-H$ stretch (~3300 cm^{-1}), $C=O$ stretch (~1700 cm^{-1}), $C-O-C$ stretch (~1100 cm^{-1}), and iodide-associated vibrations between 500 and 800 cm^{-1} for easier identification of specific chemical interactions [23, 24].

The spectroscopic alteration noticed was utilized to infer potential interactions among plasticizers, polymer, salt, and nanofiller. The incorporation of carbon black was also specifically investigated for its influence on the network of hydrogen bonding of PVA and its impacts on subsequent ionic conductivity. Such findings confirmed the development of the PVA-based GPE system and provided insight into the structural role played by carbon black as a nanofiller in enhancing the polymer matrix.

X-ray diffraction (XRD)

The XRD analysis was carried out on a PANalytical X'Pert PRO MRD PW3040 diffractometer with Cu-Kα radiation ($\lambda = 0.154\,nm$) at 40 kV and 30 mA. Diffraction patterns were scanned over a 2θ range of 5° to 55° at a consistent scan rate of 2° min^{-1} and a count time of 1s per step, which was the optimal compromise between data quality and efficiency.

The obtained diffraction spectra were analysed to determine the degree of crystallinity according to the peak sharpness and intensity, where sharp and narrow peaks indicated crystalline domains and broad peaks corresponded to amorphous regions. The crystallite size (D) was estimated using the Debye-Scherrer equation [25]:

$$D = \frac{K\lambda}{\beta \cos\theta} \tag{1}$$

where K is the Scherrer constant (0.98), λ is the X-ray wavelength (0.154 nm), and β is the full width at half maximum (FWHM).

Further analysis was dedicated to identifying the characteristic diffraction peaks of PVA, CB, KI, and I_2 and assessing the structural changes induced by CB addition as a nanofiller. Additionally, from XRD data, the degree of crystallinity (X_c) for GPE samples were observed by employing peak deconvolution method. This is the most accurate approach for polymer-based composites, as it allows to separate the ordered (crystalline) signals from the disordered (amorphous) signals. X_c was measured using equation [26]:

$$X_c = \frac{A_c}{A_T} \times 100\% \tag{2}$$

where A_c is the total crystallinity area and A_T represents the total area of the XRD (sum of the amorphous and crystalline regions) using OriginPro software.

Electrochemical impedance spectroscopy (EIS) Measurement

Electrochemical impedance spectroscopy (EIS) was conducted using an electrochemical workstation, which is HIOKI 3532-50 LCR HiTester in the frequency range of 50 Hz to 100 kHz with temperature control was maintained at room temperature (25 °C). All measurements were performed under ambient atmospheric conditions with relative humidity (RH)~50%. This experiment was designed to study the ionic conductivity and charge transfer behaviour of the PVA-based GPE. The gel electrolyte membrane was sandwiched between two stainless steel electrodes, and the setup was sealed to minimize the interference of external humidity to accurately measure bulk resistance and ionic conductivity.

An AC amplitude of 10 mV was applied to maintain the system behaviour pseudo-linear for the response to obey Ohm's law and to be modelled with certainty. Each sample allowed a stabilization time of at least 30 min prior to measurement to ensure equilibrium. The measurement was repeated for three times, and the average value was considered for the calculation of the conductivity. The impedance spectra were fitted using an equivalent circuit consisting of bulk resistance (R_b) in series with a constant phase element (CPE) and Warburg impedance (W), and the fitting was performed with nonlinear least-square optimization. This fitting procedure ensures that the reported electrochemical parameters are reliable and consistent [27–29]. The resultant impedance spectra were plotted in the form of Nyquist plots and fitted, and the R_b was identified from the intercept of the real axis at high frequency. The ionic conductivity (σ) was then calculated using the relation [30]:

$$\sigma = \frac{t}{R_b A} \tag{3}$$

where t is the electrolyte thickness 0.2 cm, R_b is the bulk resistance, and A is the stainless-steel electrode contact area 2.0106 cm^2.

Results and discussion

X-ray diffraction (XRD) Analysis

The XRD patterns of PVA-based GPEs as shown in Fig. 2 reveal that carbon black (CB) concentrations profoundly influence the structural organization of the polymer matrix. The pristine CB exhibited a sharp crystalline peak at 2θ ~ 26.39° (FWHM = 0.02 rad), within the typical 25–30° range for graphitic carbon, serving as a reference for structural changes in modified GPEs as listed in Table 2. A broad amorphous shoulder at 15–23.7° in pristine CB confirms its partial graphitic nature, typical of commercial carbon black powders.

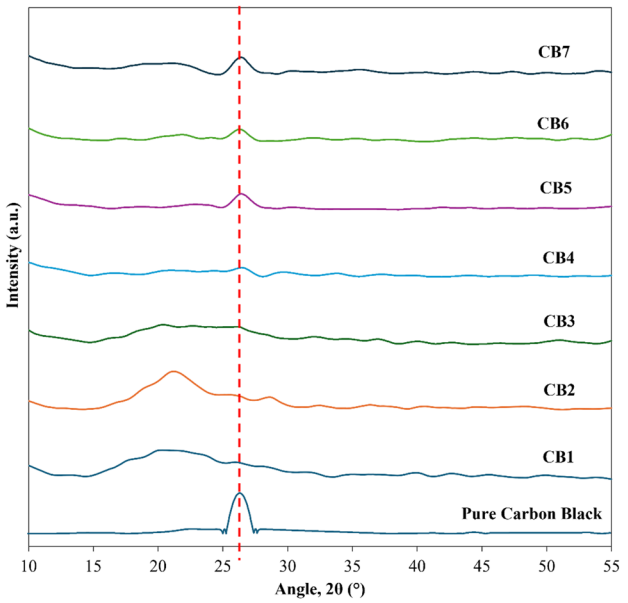

Fig. 2 XRD patterns of PVA-based GPEs with varying concentration of carbon black

Table 2 XRD parameters: peak position, FWHM, crystallite size, and degree of crystallinity

Sample	2θ (°)	FWHM (rad)	Crystallite size, D (nm)	Degree of crystallinity (X_c) (%)
Pure carbon black	26.39	0.02	6.29	48.18
CB1	21.12	0.03	4.27	63.23
CB2	20.98	0.04	3.36	68.15
CB3	25.27	0.06	2.57	47.28
CB4	24.59	0.12	1.14	31.51
CB5	26.45	0.02	8.36	45.99
CB6	26.08	0.02	8.93	49.04
CB7	26.39	0.01	10.05	52.53

From CB1 to CB4, crystallite size decreased progressively, with CB4 showing the broadest peak (FWHM = 0.12 rad) and smallest size of 1.14 nm with decreased crystallinity at 31.51%. This reflects CB's role in lowering PVA crystallinity, where at low to moderate loadings, well-dispersed CB particles disrupt heterogeneous nucleation and PVA hydrogen bonding, restricting chain folding and promote amorphous domains that favor ion transport [31]. At moderate CB loadings, CB particles facilitate the formation of percolation pathways, which enhance the connectivity of the gel network and promote efficient ion transport.

The same trends have been reported by Noer et al. [32] who observed well-dispersed CB fillers at 5 wt% in polyethylene (LDPE)-CB nanocomposites, whereas higher loadings caused agglomeration. Ungár et al. [33] also explained that the widening of the peak in CB is caused by extremely small crystallites, lattice strain, irregular particle shapes that hinder ordered stacking. Thus, CB1–CB4 demonstrate how increasing CB content promotes amorphicity in the polymer matrix.

In contrast, CB5-CB7 revealed narrower peaks (FWHM down to 0.01 rad), with small shifts towards higher 2θ values, having larger crystallites (up to 10.05 nm), and higher X_c (52.5%) which indicating enhanced crystallinity. At these higher loadings, CB particles exceed the percolation threshold and undergo significant agglomeration [34]. This transition shifts the structural contribution from filler-polymer interaction to filler-filler π-π stacking interaction. The measured increase in crystallinity therefore largely reflects graphitic stacking within CB clusters rather than improved ordering of the PVA matrix. This agglomeration is promoted by increased hydrophobicity and matrix incompatibility, where able to block the continuous ion pathways [35]. Despite pristine CB's inherent partial amorphicity, processing-induced shear or mixing promotes graphitic stacking through agglomeration-templated order, consistent with prior observations [36].

Overall, XRD information indicates that CB4 is the most amorphous formulation, whereas CB5-CB7 are comparatively more crystalline. However, crystallinity alone is not a direct proxy for ion transport. The conductivity is governed by the interplay of amorphous fraction, segmental mobility, and the connectivity of the CB network. At low to moderate CB loadings (CB1-CB4), well-dispersed CB reduces PVA crystallinity and enhances amorphicity, favoring ion transport. At higher CB loadings (CB5-CB7), CB aggregation dominates, increasing apparent crystallinity from CB cluster stacking while blocking ion pathways and reducing conductivity. This interpretation resolves the

apparent contradiction between crystallinity and conductivity seen for CB1 and CB2.

FTIR analysis

Figure 3 presents the FTIR spectra of the PVA-EC-PC-KI-CB GPE system, revealing key vibrational changes that reflect molecular interactions among the components. The spectra show reproducible, CB-dependent shifts and changes in band shapes across several vibrational regions that are consistent with altered hydrogen bonding, ion–dipole interactions, and polymer–filler interfacial effects. The broad O–H stretching band (~3300–3400 cm^{-1}) becomes progressively broader and slightly shifts toward lower wavenumbers from CB1 to CB7. This trend is consistent with an increasing fraction of PVA-OH groups participating in stronger and more heterogeneous hydrogen-bonding environments as CB content increases, plausibly involving interactions with KI anions (I^-), EC-PC carbonyls, and CB surface functionalities. These shifts are typical for PVA-based GPEs upon salt and plasticizer incorporation and reflect changes in the hydrogen-bond network density and heterogeneity, which affect segmental mobility and mechanical rigidity [37]. Thus, increasing CB content modifies the spatial distribution and strength of the PVA hydrogen bonding network, with low CB loadings reinforcing local H-bonding via CB surface groups and higher loadings introducing more heterogeneous, constrained regions due to CB aggregation. However, FTIR peak shifts alone do not uniquely identify the precise chemical partners or spatial arrangement of the hydrogen-bonded species.

In the C=O stretching region (~1770–1777 cm^{-1}) slight shifts from CB1 to CB7 indicate coordination between the carbonate groups of EC and PC and K^+ ions, as well as possible interactions with the CB surface. Such shifts are typical of K^+-containing carbonate electrolytes, which is known to stabilize ions within the polymer matrix and promote ion dissociation in K^+-containing carbonate electrolytes. The C=C stretching band of CB at ~1650 cm^{-1}, and the C=C bending region (945–952 cm^{-1}) shows minor intensity and position changes, may reflect altered electronic coupling or packing of CB domains and their interfacial contact with the polymer–plasticizer matrix [38, 39]. These changes correlate with improved CB dispersion and interfacial contact at lower loadings and more heterogeneous, aggregated interactions at higher CB content. However, FTIR alone is not sufficient to unambiguously confirm π–π or cation–π interactions.

C-H stretching (3000–2850 cm^{-1}), which arises from CH/CH_2 groups in PVA, EC, and PC, exhibits progressive broadening and subtle shifts, suggesting that alkyl and alkoxy segments experience constrained local dynamics when adsorbed on CB surfaces. This is consistent with studies on carbon black-polymer composites, in which filler surfaces restrict polymer chain mobility and alter relaxation behavior near the interface [38, 40]. Shifts in the C-O (1004–1014 cm^{-1}) and O-H bending (1404–1438 cm^{-1}) regions further indicate dynamic polymer-filler and polymer-ion interactions. The summary of the FTIR peaks for PVA-EC-PC-KI-CB system is shown in Table 3.

Thus, all the spectral shifts highlighted that the hydrogen bonding, ion-dipole interactions and van der Waals forces

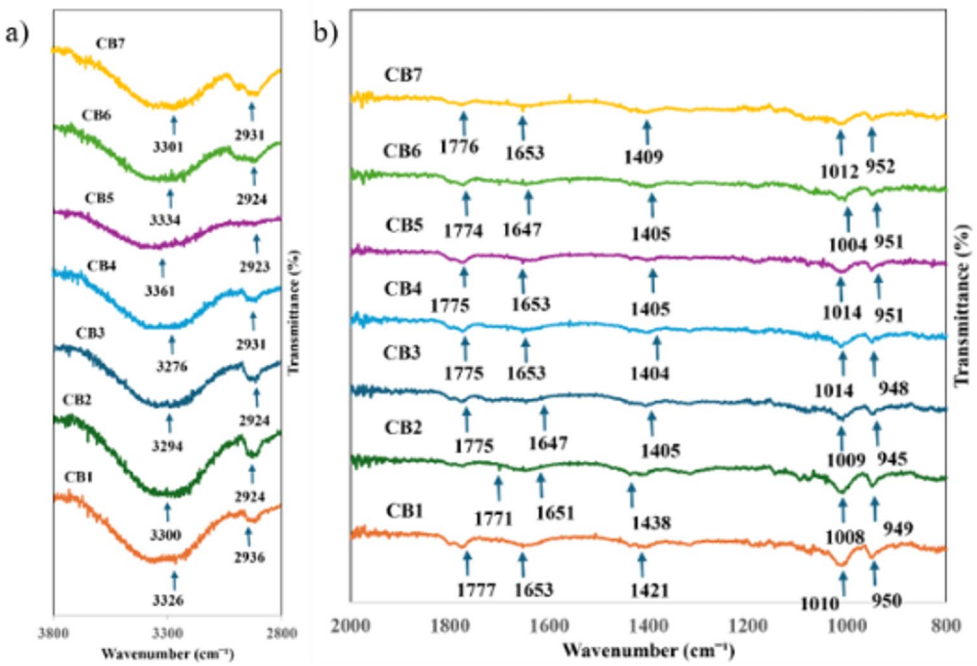

Fig. 3 FTIR spectra of PVA–EC-PC–KI–CB systems in the wavenumber range of (a) 3800 to 2800 cm^{-1} and (b) 2000 to 800 cm^{-1}

Table 3 FTIR wavenumber assignments for PVA-EC-PC-KI-CB system at varying CB concentrations

Wavenumber (cm^{-1})								Reference
Assignments	PVA-EC-PC-KI-CB							
	CB1	CB2	CB3	CB4	CB5	CB6	CB7	
O-H Stretching	3326	3300	3294	3276	3361	3334	3301	[41, 42]
C-H Stretching	2936	2924	2924	2931	2923	2924	2931	[41, 42]
C=O Stretching	1777	1771	1775	1775	1775	1774	1776	[41, 42]
C=C Stretching	1653	1651	1647	1653	1653	1647	1653	[44, 45]
O-H Bending	1421	1438	1405	1404	1405	1405	1409	[46–48]
C-O Stretching	1010	1008	1009	1014	1014	1004	1012	[49, 50]
C=C Bending	950	949	945	948	951	951	952	[42, 43, 51]

all play crucial roles in the complex gel-phase structure system of GPE. Increasing CB content will affect the balance between mechanical strength and ionic transport, providing insight into optimizing the performance of the GPE [41–43]. Figure 4 illustrates the interaction in the polymer-salt-nanofiller system.

Electrochemical impedance spectroscopy (EIS) analysis

Bulk resistance, R_b was derived from the Nyquist plots as shown in Fig. 5. The impedance spectra were fitted using an equivalent circuit consisting of bulk resistance (R_b) in series with a constant phase element (CPE) and Warburg impedance (W). As shown, all GPE samples, comprised a single inclined spike line in the low-frequency region, lacking a high-frequency semicircle. The absence of a measurable semicircle in the high-frequency region suggests that the interfacial impedance at the electrode-GPE interface is either very small compared with the bulk resistance or that the system exhibits a near-ideal diffusion-controlled response, as commonly observed in leaky capacitor-like or highly conductive gel electrolytes [52, 53]. In such systems, the impedance spectrum is dominated by the bulk resistance and low-frequency diffusion, represented by a near-vertical spike. This behavior is consistent with the relatively high ionic conductivity of the present system and implies that charge-transfer resistance does not significantly limit the overall impedance under the present measurement conditions. It can be observed that R_b increased upon incorporation of 3 wt% (CB2) due to poor CB dispersion and early agglomeration at low loading, disrupting amorphous PVA pathways. As CB content reached 12 wt% (CB5), R_b decreased via percolating conductive networks that facilitate ion transport [54]. Further addition to 15 wt% (CB6) through 18 wt% (CB7) increased R_b again, resulting CB aggregation and hinders ion pathways.

Likewise, the ionic conductivity results as shown in Fig. 6, follow the same trend and provide a direct link to the XRD observations. The CB1 which is GPE sample without CB possesses the highest absolute conductivity, (15.9 ± 0.13) mS cm^{-1}. This is due to EC-PC plasticization, which promotes KI salt dissociation and enhances ion mobility in the amorphous polymer matrix. In XRD, CB1 shows a broad amorphous signature, however, in this system without CB, the measured crystallinity is dominated by the plasticized, largely amorphous polymer matrix, and conductivity is governed primarily by amorphous fraction and plasticizer-enhanced ion mobility, not by CB-induced ordering. Adding 3 wt% (CB2) led to the significant decrease in conductivity to (1.20 ± 0.02) mS cm^{-1}, despite CB2 showing a higher degree of crystallinity and smaller crystallite size than CB1. This apparent contradiction is explained by the dispersion state and network connectivity. At this low loading, CB is poorly dispersed and begins to agglomerate, disrupting continuous polymer-ion pathways and increasing R_b. Thus, the crystallinity value alone is not the controlling factor, but the formation of blocking CB aggregates at low loading is the dominant effect.

At 6 wt% (CB3) the conductivity increases to approximately (3.50 ± 0.03) mS cm^{-1}, suggesting that a low level of well-dispersed filler can enhance the amorphous phase and segmental mobility of PVA chains, thereby improving ion mobility. Further increasing the CB content to 9 wt% (CB4), yields a conductivity of (7.50 ± 0.01) mS cm^{-1}, while the highest value among the CB-doped samples is achieved at 12 wt% (CB5) (11.80 ± 0.00) mS cm^{-1}. CB4 is the most amorphous sample as observed in XRD analysis, and its higher conductivity relative to CB2 and CB3 is consistent with well-dispersed CB reducing PVA crystallinity and enhancing amorphicity. This optimum conductivity at CB5, indicating that CB forms a partially percolated network that provides continuous low-resistance pathways while balancing polymer continuity and interfacial area [55]. Moreover, CB acts as a Lewis acid, enhancing free volume in PVA chains and improving segmental motion and ion hopping, resulting in enhance ionic conductivity. Beyond this loading, at higher loadings of 15 wt% (CB6) and 18 wt% (CB7), conductivity decreases due to CB aggregation, which obstructs ion transport channels.

These results demonstrate that the unmodified PVA-EC-PC-KI matrix (CB1) has the overall maximum across all samples, indicating this plasticized CB-free matrix attains

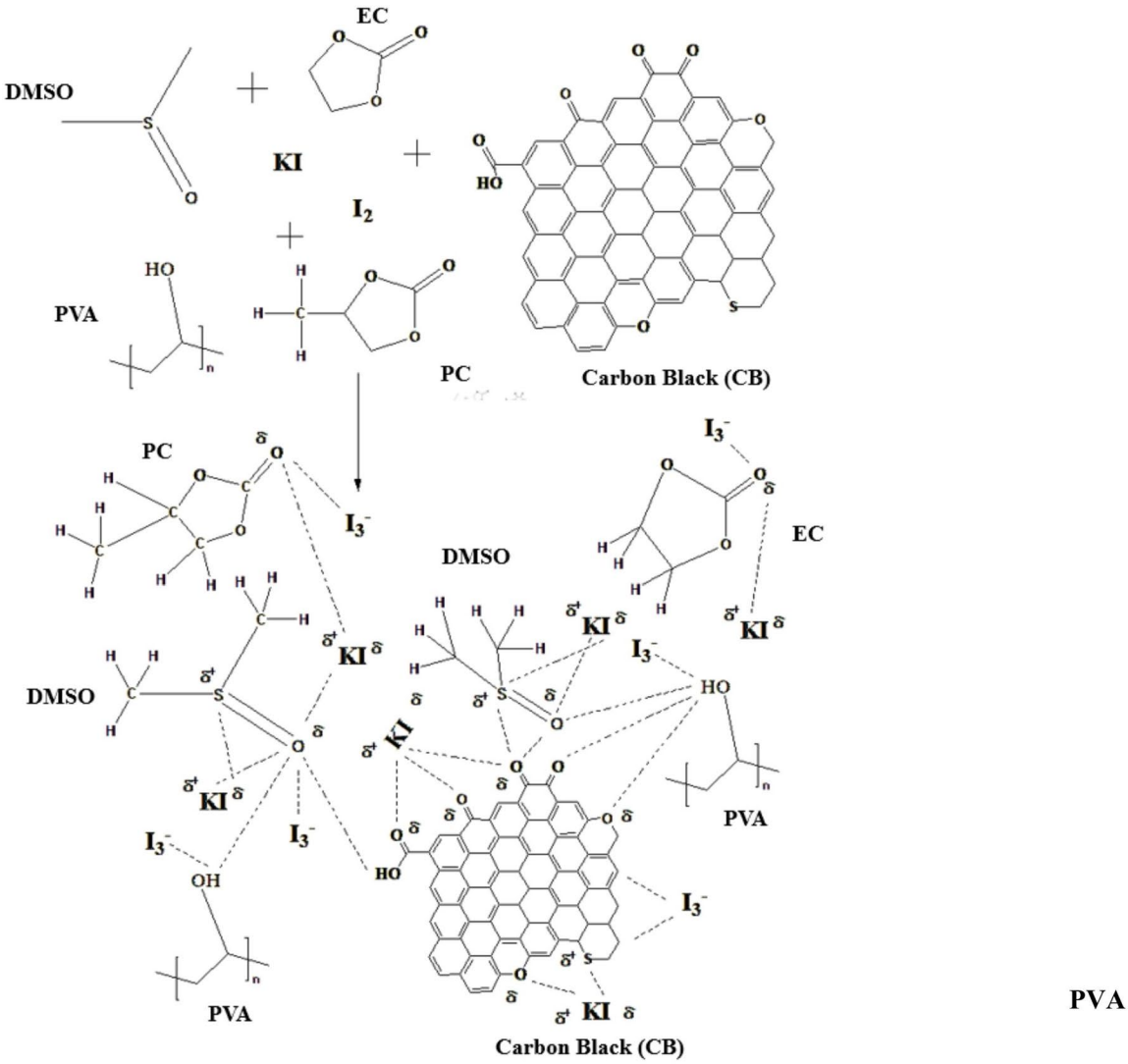

Fig. 4 Interaction in the polymer-salt-nanofiller (PVA-EC-PC-KI-CB) system

the largest amorphous fraction and greatest salt dissociation, producing maximal ion mobility. However, within the CB-doped series, CB5 yields the maximum conductivity, suggesting moderate CB loading optimizes ion transport via percolative pathways while maintaining polymer continuity. The ionic conductivity mechanism is influenced by polymer chain mobility, amorphous phase fraction, and the conductive pathways in the CB network. At low CB loadings (CB2), the filler serves as a localized plasticizer, increasing segmental motion and reducing crystallinity. At moderate, well-dispersed CB (CB3-CB5) creates a percolating network that can reduce local crystallinity and establish conductive percolation pathways that improve conductivity compared with other CB-doped samples. In contrast, high CB levels lead to aggregation, which introduces barriers and disrupts the polymer matrix continuity, ultimately restricting ion mobility and increasing bulk resistance [56]. This explanation reconciles the XRD, FTIR, and EIS observations.

The present PVA-based GPE system exhibits higher conductivity than the other polymer used with CB as nanofiller due to its excellent characteristics. The ionic conductivity of 11.80 mS cm^{-1} for CB5 exceeds the typical range reported for PVA-based GPEs ($\sim 10^{-3} - 10^{-2}$ S cm^{-1}) and is competitive with advanced PVA-nanocomposite systems. A comparison with selected literature systems is summarized in Table 4, which highlights that the present PVA-EC-PC-KI-CB GPE at 12 wt% CB achieves comparable to or higher conductivity than many PVA-based GPEs, making it suitable for applications requiring high ionic mobility. These observations suggest that CB can optimize microstructure and ion

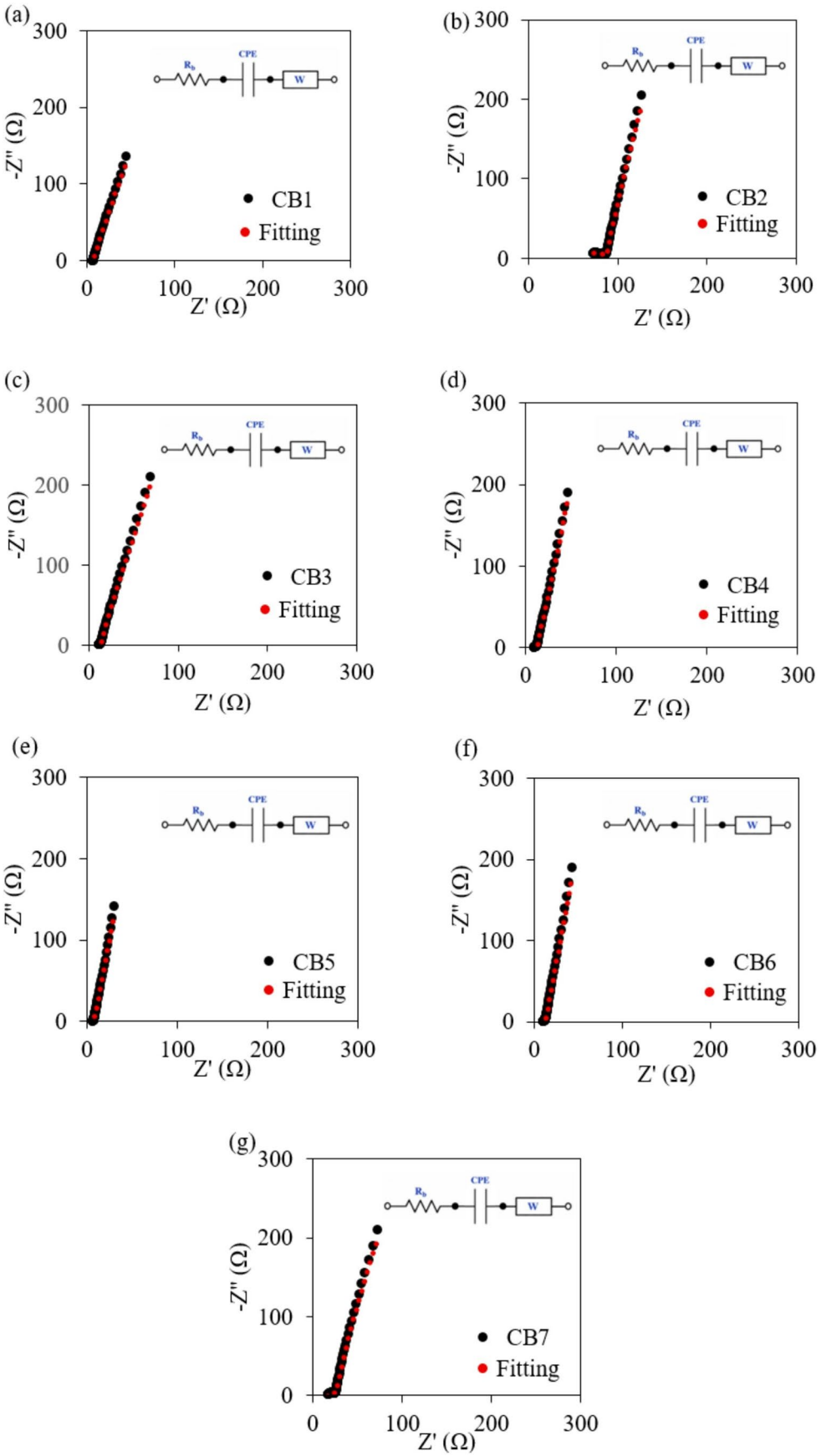

Fig. 5 The Nyquist plots for PVA-EC-PC-KI-CB GPE system

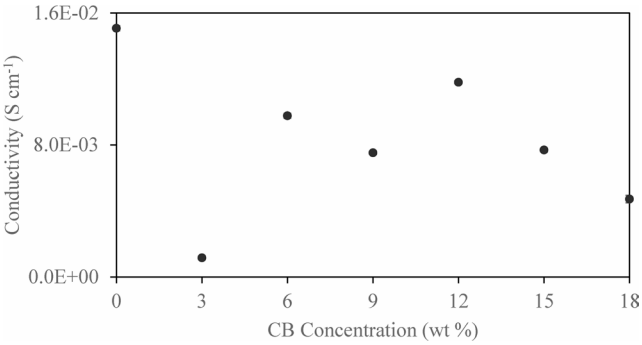

Fig. 6 Effect of CB nanofiller on conductivity

Table 4 Comparison of previous GPE system used CB as nanofiller

GPE system	CB loading (wt%)	Ionic conductivity, σ (mS cm^{-1})	Reference
PEO	0.05	0.012	[19]
PMMA-LiI -PMIMI	0.57	3.320	[57]
PVA-KOH	0.04	0.040	[58]
PVA-EC-PC-KI	12.00	11.80	Present

transport in PVA-based GPEs, although the improvement is influenced by factors such as filler concentration and dispersion quality. However, if further increased the amount of CB the ionic conductivity of GPE would be low due to CB aggregation. Overall, the present EIS analysis, combined with the ionic conductivity trends, provides a solid basis for understanding how multi-component GPEs can be optimized toward better electrochemical performance.

Conclusion

This study demonstrates that carbon black (CB) nanofiller incorporation into PVA-EC-PC-KI gel polymer electrolytes (GPEs) significantly tailors structural morphology, molecular interactions, and ionic conductivity. XRD analysis reveals optimal amorphicity at 9–12 wt% CB which its X_c down to 31.51% for CB4, disrupting PVA crystallinity to enhance ion pathways, while higher loadings induce agglomeration and graphitic reordering. FTIR confirms strengthened H-bonding and ion coordination, fostering heterogeneous networks that balance mechanical integrity and segmental mobility. Within the CB-doped series, an optimum at 12 wt% CB (CB5) produced the highest conductivity among CB-containing samples (11.80 mS cm^{-1}) by balancing reduced crystallinity and partially percolated conductive pathways. However, the highest absolute conductivity measured in this study was obtained for the pristine, plasticized electrolyte (CB1, 15.9 mS cm^{-1}). Therefore, while CB is a promising low-cost filler to tailor microstructure and ion transport, further optimization and device-level validation are required before asserting application readiness for future research on dye-sensitized solar cell (DSSC) applications.

Acknowledgements Authors thanks Universiti Sains Malaysia, Bridging Grant with Project No: R501-LR-RND003-0000002095-0000.

Author contributions A.A. wrote and edited the manuscript. C.G. prepared the gel polymer electrolytes and wrote the main manuscript text. P.Q.B. prepared the gel polymer electrolytes. A.R.M. performed the X-ray diffraction measurements. N.M. analyzed the X-ray diffraction results. M.H. obtained the Fourier-transform infrared spectroscopy results. N. measured the electrochemical impedance spectroscopy results. I.M. analyzed the electrochemical impedance spectroscopy results. M.F. and M.F. finalized the reference list. M.F. analyzed the Fourier-transform infrared spectroscopy results, edited the manuscript, and finalized it. All authors read and approved the final manuscript.

Data availability No datasets were generated or analysed during the current study.

Declarations

Competing interests The authors declare no competing interests.

References

1. Yang H, Wu N (2022) Ionic conductivity and ion transport mechanisms of solid-state lithium-ion battery electrolytes: A review. Energy Sci Eng 10(5). https://doi.org/10.1002/ese3.1163
2. Rayung M, Aung MM, Azhar SC, Abdullah LC, Su'ait MS, Ahmad A et al (2020) Bio-based polymer electrolytes for electrochemical devices: Insight into the ionic conductivity performance. Materials 13(4):838. https://doi.org/10.3390/ma13040838
3. Han L, Wang L, Chen Z, Kan Y, Hu Y, Zhang H et al (2023) Incombustible polymer electrolyte boosting safety of solid-state lithium batteries: A review. Adv Funct Mater 33(32). https://doi.org/10.1002/adfm.202300892
4. Ahmed MS, Islam M, Raut B, Yun S, Kim HY, Nam KW (2024) A comprehensive review of functional gel polymer electrolytes and applications in lithium-ion battery. Gels 10(9):563. https://doi.org/10.3390/gels10090563
5. Aruchamy K, Ramasundaram S, Divya S, Chandran M, Yun K, Oh TH (2023) Gel polymer electrolytes: Advancing solid-state batteries for high-performance applications. Gels 9(7):585. https://doi.org/10.3390/gels9070585
6. Abubakar Abdulkadir B, Setiabudi HD (2025) Progress and accomplishments in polymer blend electrolytes for electrochemical energy storage: A comprehensive review. Polymer-Plastics Technol Mater 64(14):2143–2178. https://doi.org/10.1080/25740881.2025.2511698
7. Behzadi Pour G, Nazarpour Fard H, Fekri Aval L (2024) A comparison of the electrical properties of gel polymer electrolyte-based supercapacitors: A review of advances in electrolyte materials. Gels 10(12):803. https://doi.org/10.3390/gels10120803
8. Rahim AA, Shamsuri NA, Adam AA, Aziz MF, Hamsan MH, Rusdi H et al (2024) Characterization of nanocomposite polyvinyl alcohol/cellulose acetate blend gel polymer electrolytes for supercapacitor application. J Energy Storage 97:112964. https://doi.org/10.1016/j.est.2024.112964
9. Alinejad M, Buraidah MH, Teo LP, Arof AK (2023) Saffron dye-sensitized solar cells with polyvinyl alcohol based gel polymer electrolytes. Opt Quant Electron 55(9). https://doi.org/10.1007/s11082-023-05078-z
10. Raut P, Kishnani V, Mondal K, Gupta A, Jana SC (2022) A Review on gel polymer electrolytes for dye-sensitized solar cells. Micromachines 13(5):680. https://doi.org/10.3390/mi13050680

11. Aziz MF, Rahim AA, Rais ARM (2025) Unveiling ionic conductivity and ion transport properties in polyvinyl alcohol-based gel polymer electrolytes with quaternary ammonium iodide. J Polym Mater 42(4):1097–1099. https://doi.org/10.32604/jpm.2025.071129
12. Ling CK, Aung MM, Abdullah LC, Lim HN, Uyama H (2020) A short review of iodide salt usage and properties in dye sensitized solar cell application: Single vs binary salt system. Sol Energy 206:1033–1038. https://doi.org/10.1016/j.solener.2020.06.055
13. Farhana NK, Saidi NM, Bashir S, Ramesh S, Ramesh K (2021) Review on the revolution of polymer electrolytes for dye-sensitized solar cells. Energy Fuels 35(23):19320–19350. https://doi.org/10.1021/acs.energyfuels.1c03039
14. Rahim AA, Aziz MF (2024) Ionic conductivity of PVA-based gel electrolyte containing diethyl carbonate plasticizer. Jurnal Fizik Malaysia 45:100097–110109
15. Aziz MF, Azam MA, Yusuf SNF, Buraidah MH, Arof AK (2022) Influence of potassium iodide in polyvinyl alcohol-based gel polymer electrolyte for efficiency enhancement of dye-sensitized solar cells. J Polym Res 29(11). https://doi.org/10.1007/s10965-022-03305-x
16. Kuo TR, Lin LY, Lin KY, Yougbaré S (2022) Effects of size and phase of TiO_2 in poly (vinyl alcohol)-based gel electrolyte on energy storage ability of flexible capacitive supercapacitors. J Energy Storage 52:104773. https://doi.org/10.1016/j.est.2022.104773
17. Fan X, Liu J, Song Z, Han X, Deng Y, Zhong C, Hu W (2019) Porous nanocomposite gel polymer electrolyte with high ionic conductivity and superior electrolyte retention capability for long-cycle-life flexible zinc–air batteries. Nano Energy 56:454–462. https://doi.org/10.1016/j.nanoen.2018.11.057
18. Luo Y, Shi Z, Qiao S, Tong A, Liao X, Zhang T, Bai J, Xu C, Xiong X, Chen F, Xu W (2024) Advances in nanomaterials as exceptional fillers to reinforce carbon fiber-reinforced polymers composites and their emerging applications. Polym Compos 46(1):54–80. https://doi.org/10.1002/pc.29027
19. Negi SS, Rawat S, Singh PK, Savilov SV, Yadav T, Yahya MZA, Chandra SR (2024) Conducting carbon black nano-filler doped polymer electrolyte for electrochemical application. Chem Select 9(25). https://doi.org/10.1002/slct.202400847
20. Pal B, Yang S, Ramesh S, Thangadurai V, Jose R (2019) Electrolyte selection for supercapacitive devices: a critical review. Nanoscale Adv 1(10):3807–3835. https://doi.org/10.1039/c9na00374f
21. Gamal R, Sheha E, El Kholy MM (2023) Dimethyl sulfoxide as a function additive on halogen-free electrolyte for magnesium battery application. RSC Adv 13(18):11959–11966. https://doi.org/10.1039/d3ra01707a
22. Al-Kelani M, Buthelezi N (2024) Advancements in medical research: Exploring Fourier transform infrared (FTIR) spectroscopy for tissue, cell, and hair sample analysis. Skin Res Technol 30(6). https://doi.org/10.1111/srt.13733
23. Rong Z, Henry BR, Robinson TW, Kjaergaard HG (2005) Absolute Intensities of CH Stretching Overtones in Alkenes. The Journal of Physical Chemistry A 109(6):1033–1041. https://doi.org/10.1021/jp040639f
24. Lin SY, Cheng WT, Wei YS, Lin HL (2011) DSC-FTIR microspectroscopy used to investigate the heat-induced intramolecular cyclic anhydride formation between Eudragit E and PVA copolymer. Polym J 43(6):577–580. https://doi.org/10.1038/pj.2011.15
25. Fatimah S, Ragadhita R, Husaeni DFA, Nandiyanto ABD (2021) How to calculate crystallite size from x-ray diffraction (XRD) using Scherrer method. ASEAN J Sci Eng 2(1):65–76. https://doi.org/10.17509/ajse.v2i1.37647
26. Ali NM, Kareem AA (2022) Ionic conductivity enhancement for PVA/20wt.% $CuSO_4$ gel polymer electrolyte by using glycerin. Chalcogenide Lett 19(3):217–225. https://doi.org/10.15251/cl.2022.193.217
27. Chikkatti BS, Sajjan AM, Banapurmath NR (2023) The state of understanding of the electrochemical behaviours of a valve-regulated lead–acid battery comprising manganese dioxide-impregnated gel polymer electrolyte. Mater Adv 4(23):6192–6198. https://doi.org/10.1039/d3ma00563a
28. Chikkatti BS, Sajjan AM, Banapurmath NR, Ayachit NH, Jazaa Y, Yunus Khan TM, Umarfarooq MA (2025) Novel polymer gel electrolytes comprising montmorillonite embedded in sodium alginate and their electrochemical performance for future lead acid batteries. New J Chem 49(9):3654–3660. https://doi.org/10.1039/d4nj05557h
29. Chikkatti BS, Sajjan AM, Banapurmath NR (2026) The recent research progress and the prospect of gel polymer electrolytes in valve-regulated lead acid battery. J Power Sources 662:238769. https://doi.org/10.1016/j.jpowsour.2025.238769
30. Aziz MF, Rahim AA, Razak ESA, Jaaffar SNA, Buraidah MH, Shukur MF (2025) Enhanced ion transport and structural dynamics in gel polymer electrolytes containing a plasticizer prospect for DSSC application. Ionics 31(6):6103–6115. https://doi.org/10.1007/s11581-025-06270-9
31. Cheong JY, Koay JSC, Gopal SR, Velayutham TS, Gan WC (2025) Enhancing the tribopositive characteristics of polyvinyl alcohol (PVA)-carbon composites by optimizing the PVA-carbon interaction with various carbon fillers. Nanoscale Adv 7(3):819–829. https://doi.org/10.1039/d4na00820k
32. Noer Z, MN N, Bukit N, Juwairiah, Susilawati (2018) Ikhwanuddin. Characterization of low-density polyethylene (LDPE)/carbon black (CB) nanocomposite-based packaging material. Journal of Physics: Conference Series 1120(1):012066. https://doi.org/10.1088/1742-6596/1120/1/012066
33. Ungár T, Gubicza J, Tichy G, Pantea C, Zerda TW (2004) Size and shape of crystallites and internal stresses in carbon blacks. Compos A Appl Sci Manuf 36(4):431–436. https://doi.org/10.1016/j.compositesa.2004.10.017
34. Payandehpeyman J, Mazaheri M, Zeraati AS, Shahriar, Jamasb (2023) Uttandaraman Sundararaj. Physics-Based Modeling and Experimental Study of Conductivity and Percolation Threshold in Carbon Black Polymer Nanocomposites. Appl Compos Mater 31(1):127–147. https://doi.org/10.1007/s10443-023-10169-x
35. Cattaruzza M, Fang Y, István Furó, Lindbergh G, Liu F, Johansson M (2025) Hybrid polymer–liquid lithium ion electrolytes: Effect of carbon black during polymerization-induced phase separation. Polymer 326:128341. https://doi.org/10.1016/j.polymer.2025.128341
36. Zhang S, Cui Y, Wu B, Song R, Song H, Zhou J et al (2013) Control of graphitization degree and defects of carbon blacks through ball-milling. RSC Adv 4(1):505–509. https://doi.org/10.1039/c3ra44530e
37. Ni Q, Ye W, Du M, Shan G, Song Y, Zheng Q (2022) Effect of hydrogen bonding on dynamic rheological behavior of PVA aqueous solution. Gels 8(8):518. https://doi.org/10.3390/gels8080518
38. Buaksuntear K, Kohl P, Li Y, Smitthipong W (2025) Improvement of carbon black dispersion in mussel-Inspired composites from epoxidized natural rubber using aromatic interactions. ACS Appl Polym Mater 7(6):3576–3587. https://doi.org/10.1021/acsapm.4c03648
39. Singh C, Shukla P, Agrawal S (2020) Ion transport studies in PVA: NH_4CH_3COO gel polymer electrolytes. High Perform Polym 32(2):208–219. https://doi.org/10.1177/0954008319898242
40. ALjubouri F, Kadhim Jawad M (2023) FTIR and electrical behavior of blend electrolytes based on (PVA/PVP). Iraqi J Phys 21(1):1–9. https://doi.org/10.30723/ijp.v20i1.1093
41. Alzahrani HAH (2022) CuO and MWCNTs nanoparticles filled PVA-PVP nanocomposites: Morphological, optical, dielectric, and electrical characteristics. IntechOpen eBooks 32(5). https://doi.org/10.5772/intechopen.105810

42. Chen J, Liu B, Gao X, Xu D (2018) A review of the interfacial characteristics of polymer nanocomposites containing carbon nanotubes. RSC Adv 8(49):28048–28085. https://doi.org/10.1039/c8ra04205e
43. Tareen MHK, Hussain F, Zubair Z, Aslam S, Saleem T, Awais M et al (2022) Effects of carbon black on epoxidized natural rubber composites: Rheological, abrasion, and mechanical study. J Compos Mater 56(29):4473–4485. https://doi.org/10.1177/00219983221134512
44. Fang B, Wang T, Chen X, Jin T, Zhang R, Zhuang W (2015) Modeling vibrational spectra of ester carbonyl stretch in water and DMSO based on molecular dynamics simulation. J Phys Chem B 119(38):12390–12396. https://doi.org/10.1021/acs.jpcb.5b06541
45. Chauhan APS, Chawla K (2016) Comparative studies on graphite and carbon black powders, and their dispersions. J Mol Liq 221:292–297. https://doi.org/10.1016/j.molliq.2016.05.043
46. Manikandan KM, Arunagiri Yelilarasi, Saravanakumar SS, Althomali RH, Khan A, Abualnaja KM et al (2021) The effect of plasticizers on the polypyrrole-poly(vinyl alcohol)-based conducting polymer electrolyte and its application in semi-transparent dye-sensitized solar cells. Membranes 11(10):791. https://doi.org/10.3390/membranes11100791
47. Basha SKS, Sundari GS, Kumar KV (2016) Studies on electrical properties of potassium acetate complexed with polyvinyl alcohol for electrochemical cell applications. Mater Today: Proc 3(1):11–20. https://doi.org/10.1016/j.matpr.2016.01.109
48. Song L, Sun S, Zhao X (2023) Ethylene carbonate plasticized polymer electrolyte for chloride ion batteries with enhanced reversible capacity. Solid State Ionics 399(116314):116314. https://doi.org/10.1016/j.ssi.2023.116314
49. Liu Q, Zhao Y, Gao S, Yang X, Fan R, Zhi M et al (2021) Recent advances in the flame retardancy role of graphene and its derivatives in epoxy resin materials. Compos Part A: Appl Sci Manufac 149(106539):106539. https://doi.org/10.1016/j.compositesa.2021.106539
50. Smith BC (2022) The infrared spectra of polymers, VI: Polymers with C-O bonds. Spectroscopy 37(5):15–19. https://doi.org/10.56530/spectroscopy.ly3071f5
51. Fredi G, Zimmerer C, Scheffler C, Pegoretti A (2020) Polydopamine-coated paraffin microcapsules as a multifunctional filler enhancing thermal and mechanical performance of a flexible epoxy resin. J Compos Sci 4(4):174. https://doi.org/10.3390/jcs4040174
52. Patel M, Mishra K, Chaudhary NA, Madhani V, Chaudhari JJ, Kumar D (2024) A sodium ion conducting gel polymer electrolyte with counterbalance between 1-ethyl-3-methylimidazolium tetrafluoroborate and tetra ethylene glycol dimethyl ether for electrochemical applications. RSC Adv 14(20):14358–14373. https://doi.org/10.1039/d4ra01615g
53. Aziz S, Abdullah R, Rasheed M, Ahmed H (2017) Role of ion dissociation on DC conductivity and silver nanoparticle formation in PVA:AgNt based polymer electrolytes: Deep insights to ion transport mechanism. Polymers 9(12):338. https://doi.org/10.3390/polym9080338
54. Negi SS, Rawat S, Singh PK, Pandey SP, Yadav T, Srivastava M, Singh RC (2024) Influence of carbon black on conductivity and structure of polyethylene oxide based polymer electrolyte film. Macromolecular Symposia 413(1):2300104. https://doi.org/10.1002/masy.202300104
55. Wang Y, Zhang B, Mao M, Cao L, Mohamad AA, Alshoaibi AA, Abdurakhmanov G, Lou X, Wang D, Song K (2025) Optimization strategies of filler morphology and spatial design in polymer nanocomposites for next-generation energy storage. J Adv Dielectr 15(03). https://doi.org/10.1142/s2010135x25300014
56. Brunella V, Rossatto BG, Mastropasqua C, Cesano F, Scarano D (2021) Thermal/electrical properties and texture of carbon black PC polymer composites near the electrical percolation threshold. J Compos Sci 5(8):212. https://doi.org/10.3390/jcs5080212
57. Mohan K, Swapnil Dolui, Nath BC, Bora A, Sharma S (2017) Swapan Kumar Dolui. A highly stable and efficient quasi solid-state dye sensitized solar cell based on polymethyl methacrylate (PMMA)/carbon black (CB) polymer gel electrolyte with improved open circuit voltage. Electrochim Acta 247:216–228. https://doi.org/10.1016/j.electacta.2017.06.062
58. Barzegar F, Dangbegnon JK, Bello A, Momodu DY, Johnson AT, Manyala N (2015) Effect of conductive additives to gel electrolytes on activated carbon-based supercapacitors. AIP Adv 5(9). https://doi.org/10.1063/1.4931956